Development of an ultrasensitive label-free immunosensor for fungal aflatoxin B1 detection

Zeineb Ben Abdallah, Christine Grauby-Heywang, Laure Béven, Sébastien Cassagnere, Fabien Moroté, Eddie Maillard, Halim Sghaier, Touria Cohen Bouhacina

Development of an ultrasensitive label-free immunosensor for fungal aflatoxin B1 detection

Zeineb BEN ABDALLAH[(a, b)], Christine GRAUBY-HEYWANG[(a)], Laure BEVEN[(c)], Sebastien CASSAGNERE[(a)], Fabien MOROTÉ[(a)], Eddie MAILLARD[(a)], Halim SGHAIER [(b)], Touria COHEN BOUHACINA [(a)]*

a Univ. Bordeaux, CNRS, LOMA, UMR 5798, 351 cours de la Libération, 33400 Talence, France

b Université de Monastir, Faculté des Sciences de Monastir, 5019, Monastir, Tunisie

c Univ. Bordeaux, INRA, UMR 1332 Biologie du Fruit et Pathologie, 33140 Villenave d'Ornon, France

*Corresponding author: Tel : +33 5 40 00 84 08

E-mail address: touria.cohen-bouhacina@u-bordeaux.fr

Abstract

In this work, we developed and characterized a homemade electrochemical immunosensor for the detection of fungal B1 aflatoxin (AFB1), one of the most dangerous toxins met in food production chains, for which highly specific, rapid, easy to use and low-cost detection tools are still required. Our sensor is based on screen-printed electrodes, the working one being submitted to a cleaning procedure, before being functionalized using three different protocols by a supramolecular architecture made of a streptavidin layer immobilizing biotinylated anti-AFB1 antibodies. Each step of the sensor design was studied using complementary methods (atomic force microscopy, contact angle measurement, electrochemical impedance spectroscopy, Fourier-Transform InfraRed spectroscopy and cyclic voltammetry), leading to the choice of one of the three functionalization protocols combining reproducibility and simplicity of execution for the elaboration of the final sensor. This optimized sensor allows the detection of AFB1 in a large linear range from 50 fg/ml to 5 ng/ml with a limit of detection of about 50 fg/ml, showing, therefore, a significant enhancement of sensitivity as compared to other sensors described in the literature for the detection of this toxin.

Keywords: aflatoxin AFB1, microchip, electrochemical detection, immunosensor, self-assembly

1. Introduction

Agri-food industry is considered as the main sector influenced by the spread of foodborne pathogens throughout the production chain whether on-farm, in distribution packaging or even during processing and commercialization [1]. Poor detection of such pathogenic micro-organisms by food producers can have serious consequences [2]. This issue is not limited to micro-organisms, since the detection of toxins remains in many countries also a serious concern, that needs to be urgently addressed [2-3]. In this context, aflatoxins (AF) aresecondary metabolites produced by filamentous fungi such as *Aspergillus flavus* and *A. parasiticus* commonly found as contaminants of a large variety of food and feedstuffs. Environmental factors responsible for their production include the use of fungicides or fertilizers combined with the meteorological conditions such as high temperature and humidity [4]. AFs which are present in a large variety of daily life products such as peanuts, maize, cottonseeds and tree nuts can cause both acute and chronic adverse effects on human health [5-7]. These toxins are divided into different subtypes, the most economically important being AFB1 considered as the most recurrent and harmful toxin found in peanuts and seeds [8]. At last, according to the International Agency for Research on Cancer (IARC), levels of AFs contamination in edible products range from 0.1 µg/kg to 10 µg/kg, while strict maximum concentrations have been established in 2010 by the European Commission at 2 µg/kg for AFB1 and 4 µg/kg for total AF in the case of cereals and nuts in a context of direct human consumption [9].

Conventional methods used for toxin detection such as immunoassays (for instance enzyme-linked immunosorbent assay ELISA), thin layer chromatography (TLC) and high performance liquid chromatography (HPLC) happen to be expensive, laborious, time consuming and require intervention of experts [6]. Facing major health issues, environmental and agri-food sectors must now integrate more advanced analytical techniques for more efficient routine analysis and diagnosis [3]. The detection tools must be highly specific, easy to use and low-cost and must provide a fast response (ideally in real time). In the case of low molecular weight fungal toxins such as AFB1 direct detection also often leads to the production of weak signals, justifying the development of indirect competitive immunoassays [10]. Nevertheless, more appropriate approaches and techniques have been developed for many years for the detection of low-molecular-weight molecules. This is for instance the case of a sensitive aptasensor developed for the detection of AFB1, based on the catalytic effect of aptamer/G-quadruplex DNAzyme probe, revealing furthermore high sensitivity with a detection limit at 0.02 ng/mL [11]. Another sensor was proposed based on the development of a rapid surface plasmon resonance chip

sequentially modified with cysteine-protein G, AFB1 antibody, and bovine serum albumin (BSA) [12]. Competitive assays showed detection limits of about 2.51 ng/ml in several real samples such as peanuts, rice and almonds. Another recent study described in [13] was based on the development of a multiplex Lateral Flow Immunoassay using a simple test line and an alloy of gold nanoparticles as signal reporters for the detection of fungal toxins in wheat-based foods. These systems showed a reproducible detection with clear cut-off levels at 1 ng/ml and 50 ng/ml for AFB1 and type B fumonisins, respectively, based on the specific color code of gold nanoparticles once linked with antibodies.

In parallel efforts have been made to facilitate and shorten heavy processes, leading to new tools fulfilling different conditions such as portability and ability to perform *in situ*, *in vitro* or *in-vivo* instant response tests [7]. In particular, the combination of several disciplines such as microelectronics and biology has led to the emergence of new technologies including nano-systems and lab-on-chips, to meet the needs of the market [14-19].

Today, the design of electronic noses or tongues, origami based sensors, Micro Electro Mechanical Systems (MEMs) or lab-on-chips has become a growing field thanks to new manufacturing techniques such as lithography, chemical evaporation deposition (CVD), physical evaporation deposition (PVD), 3D printing, and screen-printing [20, 21]. Among all these methods of microfabrication, screen-printing is the most exploited, especially in the last ten years, because of its ease of handling, its bulk production capacity and its adaptability. Indeed, it is possible to deposit nanoscale sensitive films in thickness on different substrates of the rigid type to the flexible and stretchable type. In addition, screen-printed sensors have undergone a great revolution over the past decade thanks to the integration of new complexes and alloys such as carbon nanotubes, nanoparticles, nano-rods and quantum dots. All these nanostructures promote the transfer of electrons in well-guided channels, facilitating the displacement of charges in a guided manner with effective kinetic properties [22, 23].

In this context, several companies have manufactured and marketed screen-printed sensors combined with several gadgets such as wireless potentiostats for electrochemical measurements in mobile applications for chemical detection and bio-detection. However, they have a limited lifetime, and their compatibility with different electronic systems is, also, limited. Compatibility issues have been solved by developing interfaces and systems that interact with commercial potentiostats, another possibility being to design their own hardware [22, 24]. They help

provide portable and miniature potentiostats, but they are still unaffordable, especially in underdeveloped countries.

In this work, we assembled a newly homemade electrochemical lab-on-chip whose electronic system performs voltammetric measurements to detect AFB1 as a target molecule. The microchip was based on a gold working electrode, chosen for its specificity and high affinity in functionalization processes by self-assembly techniques. Different physicochemical steps of surface functionalization were carried out in order to elaborate a simple but effective architecture based on the interaction between streptavidin and the biotinylated anti-AFB1 antibody, finally leading to a label-free immunosensor. In a first part, each step of functionalization was characterized and optimized using electrochemical measurements (cyclic voltammetry CV and electrochemical impedance spectroscopy EIS) coupled with complementary methods, such as Atomic Force Microscopy (AFM) and Fourier Transform-InfraRed (FTIR) spectroscopy. This allowed us to determine the most appropriate functionalization process prior to adsorption of streptavidin, followed by the immobilization of a biotinylated anti-AFB1 antibody. In a second part, electrochemical detection of AFB1 was carried out, and the sensitivity of the sensor was characterized.

In addition to effective detection of AFB1, our homemade electrochemical sensor has the advantage of being miniaturized, portable and possibly applied to other target molecules by simply changing the antibody. Moreover, it requires small detection volumes of about 1-2 µl, which is economically advantageous. At last, screen-printing technology used to build this sensor is known for its rapidity, ease-to-use, low cost and bulk production.

2. Material and methods

2.1 Reagents and chemicals

- Screen-printing process: 65:35 Silver/Silver chloride-filled flexible resin material, 8836 gold paste and RS12111 carbon resistor were from ESL Electrosciences (Berkshire, England). Alumina sheets (Al_2O_3 96%, dimensions 48.6 x 47.4 x 0.5 mm) were purchased from ELMITECH (Rungis, France).
- Cleaning, functionalization, characterizations: Cysteamin (CA), Tris buffer saline (TBS), streptavidin (SA) from *Streptomyces avidinii*, bovine serum albumin (BSA), aflatoxin B1 (AFB1) from *Aspergillus flavus,* potassium hexacyanoferrate III ($K_3Fe(CN)_6$), potassium hexacyanoferrate II trihyadrate ($K_4Fe(CN)_6.3H_2O$),

chloroform and ethanol (both HPLC grade), *N*-hydroxysuccinimide (NHS) and *N*-ethyl-*N'*-(3-dimethylaminopropyl) carbodiimide hydrochloride (EDC) were purchased from Sigma-Aldrich, France. Biotin labeled anti-AFB1 (Biotin_Anti-AFB1) monoclonal antibody was purchased from Thermofisher, France. H_2O_2 was purchased from a local pharmacy. All solutions were prepared with Millipore ultrapure water (pH 5,6, resistivity higher than 18,2 MΩ.cm).

2.2 Apparatus

2.2.1 Home-made lab-on-chip

Screen-printing was performed using the C890 setup from AUREL AUTOMATION S.P.A. (Modigliana, Italy) on alumina substrates. Pastes were deposited in the following order: gold one (working electrode, 800 °C, 30 min); Ag/AgCl (reference electrode, 150 °C, 15 min), carbon (counter electrode, 200°C, 2 hours). After each step, a heat treatment ensured the solidity of the deposit and the absence of overflow.

As shown in Figure 1a, the design of the miniaturized screen-printed microchip consists of two identical sensors that can help to, simultaneously, perform separate measurements, allowing in the same test the detection of different species in a specific way depending on the functionalization [25].

We associated the microchip with a polydimethylsiloxane (PDMS) static microfluidic cell for the statistical analysis (Figure 1b). This combination makes it possible to carry out measurements with very small volumes not exceeding 2µl.

For acquisition of the electrochemical signal, the microchip was integrated in a brass cell-test based on pogo pins connectors to ensure the connection between the sensor and the electronic system. After fabrication and dicing, the micro sensors were encapsulated using plastic envelops to protect them from dust.

2.2.2 Pretreatment of the gold electrode: cleaning process

Ambient environmental contaminants may affect the sensor response [26]. As a result, electrodes were cleaned by immersion in a mix of H_2O_2 (3%) and ethanol (2:1 ml) for 15 min. Then they were rinsed with ultrapure water and dried under a stream of nitrogen. To guarantee the performance and the reproducibility of the cleaning protocol, five different sensors were

processed and characterized by different methods (see below). In addition, for subsequent measurements, the cleaned electrode was taken as the bare reference state.

2.2.3 Functionalization protocols

The immobilization process was mainly based on the well-known streptavidin-biotin interaction [27]. Due to the high affinity of this non-covalent interaction, the streptavidin-biotin complex is unaffected by multiple washes, pH changes, or even by the presence of some chaotropic agents [28]. In this study, we used a first functionalization protocol already described in the literature for the immobilization of proteins [19]. Two other protocols have also been evaluated for their efficiency in producing sensors with a reproducible and stable response:

- Protocol 1 (Figure 2a) is based on the immobilization of streptavidin through covalent sulfur bonds provided by cysteamin. A drop (1 µl) of a 100 mM ethanolic solution of cysteamin was deposited on the surface of the working electrode for 4 h. Meanwhile, a solution containing streptavidin (50 µg/ml), EDC (2 mM) and NHS (5 mM) was freshly prepared in sodium acetate and mixed for 1h. After having rinsed the gold electrode with ultrapure water, it was dried at room temperature (20°C), and then, incubated with 1µl of modified streptavidin solution for 2h.
- Protocol 2 (Figure 2b) is similar to the previous one without the step involving cysteamin.
- Protocol 3 (Figure 2c) consists of a simple and direct adsorption of unmodified streptavidin on the gold surface. The streptavidin concentration was increased to 100 µg/ml and the electrode surface was incubated with 1 µl of this solution for 2h.

Finally, regardless of the previous procedure, the electrode was rinsed with ultrapure water, dried at room temperature and finally incubated in a solution of biotin anti-AFB1 antibody at 75 µg/ml in TBS for 2 hours, in order to couple streptavidin and biotin. A final incubation in a BSA solution (1%) for 1 hour enabled to block the unbound sites.

2.2.4 Preparation of real samples

In order to evaluate the performance of the sensor in complex environments, we injected different concentrations of AFB1 in treated rice milk samples purchased from a local market

(Bordeaux, France). Samples were processed in the same way as raw animal milk samples [29], being centrifuged at 5000 rpm for 10 min (22°C). After dissociating the different layers, known concentrations AFB1 were spiked in the liquid part. Subsequent dilutions were made using liquid phases obtained with non-contaminated milk samples.

2.3 Methods

2.3.1 Surface characterization

Characterization of the surface was necessary to monitor the quality of the paste deposition process used to design the working electrode of the sensor (before and after the cleaning process), the presence of chemical linkers and the morphological organization of our active surfaces after the different functionalization steps. Consequently, different techniques have been used:

- Atomic Force Microscopy (AFM): measurements were carried out with a Multimode AFM (Veeco-Brucker, Santa Barbara, CA) operating with a Nanoscope III.a and a Bioscope II mounted on an IX71 Olympus inverted optical microscope coupled to a NanoScope V controller, in tapping mode. Silicon cantilevers with a spring constant around 40 N/m were used. Images were obtained with a scan rate between 0.1 and 0.7 Hz. Data presented below are representative of those obtained with 12 samples (6 samples before cleaning and 6 others after treatment).
- Contact angle measurements: they were performed using a Drop Shape Analyzer (Krüss, Hamburg, Germany) in the sessile drop configuration. Results presented below are the average of measurements obtained with at least 3 different sensors, 3 drops of water (3 µl) being deposited on each sample.
- FTIR spectroscopy: spectra were used to check the presence of chemicals on samples at each functionalization steps. Data were obtained with a Perkin Elmer Frontier spectrometer in a wave range between 2600 and 3000 cm^{-1}.

2.3.2 Electrochemical measurements

For electrochemical measurements, we used our homemade electronic system previously described in [30], which performs cyclic voltammetry and chronoamperometry measurements. For all CV measurements, we used the redox couple $K_4[Fe(CN)_6]^{3-}$/ $K_4[Fe(CN)_6]^{4-}$ (10mM) in

a TBS solution (pH=7.4) as electrochemical probe amplification signal. Electrochemical measurements were performed at a scan rate of 0.1V/s and in a potential window of [-0.4 / +0.6 V] adapted to the redox couple.

EIS is an ultrasensitive and a non-destructive technique widely used for the construction and the analysis of the electrochemical interface (electrode/ electrolyte) [31, 32]. It is based essentially on the measurement of the bulk and the interfacial electrical properties of the electrochemical system., quantitative information can be extracted from these measurements such as the electrolyte resistance (Rs), the adsorbed quantity of the species fixed on the electrode, the interfacial charge transfer resistance (Rtc) as well as the mass transport on both low and high frequencies [32].EIS measurements were conducted using a PalmSens 4.0 Potentiostat / Galvanostat / Impedance Analyzer (PalmSens Compact Electrochemical Interfaces, The Netherlands) and 4 independent sensors for each protocol. Data were recorded on a frequency range between 50 mHz and 1 KHz with a potential for our surface of about 220 mV, and using the redox couple $K_4[Fe(CN)_6]^{3-}$/ $K_4[Fe(CN)_6]^{4-}$ (10mM) in a TBS solution (pH=7.4).

The detection of aflatoxin was performed using a solution of the AFB1 antigen diluted in chloroform [33] at different concentrations ranging from 50 fg/ml to 10 ng/ml, the intermediate concentrations being obtained by 10-fold serial dilutions.

3. Results and discussion

3.1 Microsensor characterization after cleaning

Figure 3a shows the current-voltage (CV) curves obtained with a gold electrode in contact with the redox couple solution before and after the cleaning process. This process induces drastic changes in the CV curve: the signal is amplified by more than 200%, indicating that the working surface becomes less resistive compared to before cleaning. This increase in current is associated with a decrease in the potential difference (ΔE) between the oxidation and reduction peaks (Figure 3b), in agreement with a previous study comparing different cleaning processes

[26]. Such observations may be associated with the removal of contaminating elements at the surface, correlated to a more electrochemically active surface [26].

In parallel with the electrochemical characterization, the contact angle measurements show a significant decrease in the contact angle of water drops from (90 ± 2)° to (50 ± 2)°, after applying the cleaning process, showing an increase of the wettability. As previously this effect can be assigned to the removal of contaminants from the surface of the electrode.

AFM imaging also reveals changes in the morphology of the electrode surface after cleaning. Before cleaning, the electrode surface is not regular with the presence of aggregates (Figure 4a and 4b). Overall, the cleaning process induces an increase of the number of aggregates and the appearance of smaller islands (Figure 4c and 4d), similar to those that could be expected in case of erosion. This observation is confirmed by an increase of the surface roughness as shown in the histograms of Figure 4e.

This erosion affecting surface organization and increasing its roughness allows the exposure of more active sites, and thus the enhancement of the charge transfer on the gold surface as observed in Figure 3a.

3.2 Assessment of the biotin anti-AFB1 antibody immobilization

Figure 5 shows the CV curves obtained with gold electrodes functionalized according to the three methods described above. While applying the protocol 1 (Figure 5a), the incubation of the gold electrode in the cysteamin solution systemically induces a decrease of both oxidation and reduction currents with respect to the bare electrode, showing an increased resistivity because of the cysteamin deposition. On the contrary, the following incubation with the streptavidin solution leads to irregular results, with either an increase or a decrease of the two currents (case of an increase in currents shown in Figure 5a). Moreover, addition of biotinylated anti-AFB1 antibody induces no modification of the CV curves, which makes it possible to conclude that these antibodies do not bind the surface. These observations prompted us to modify the functionalization procedure by eliminating the step involving cysteamin.

The response of the functionalized electrode following the second protocol (Figure 5b) was reproducible, first showing an increase in the oxidation and reduction currents and in the potential gap after deposition of the streptavidin layer, and on the other hand a decrease in currents upon binding of the biotinylated anti-AFB1 antibody.

Using protocol 3 (Figure 5c), a decrease in oxidation and reduction currents was observed when streptavidin was deposited directly on the gold surface after two hours of incubation. This indicates that streptavidin adsorbs on the surface of the electrode despite the absence of linker, forming a resistive and stable layer as previously shown in the case of its adsorption ongold nanoparticles [34]. The presence of the second antibody layer slightly increased the sensor response. Such an effect has also been observed in the case of anti-AFB1 antibodies grafted to electrodes previously functionalized with nanoparticles, the molecular architecture at the surface acting as an "electron transfer-accelerating layer" [35].

In order to confirm previous results, EIS measurements were performed. EIS Nyquist plots obtained at each functionalization step for the three protocols are shown in Figure 5. In all cases, plots are close to semicircles for bare gold electrode, the radius of these circles being proportional to the charge transfer resistance. The functionalization of electrodes leads to different changes on these plots according to the protocol.

In the case of protocol 1 (Figure 5d), adding the following layer of cysteamin induces a strong decrease of the resistance as shown by the very small radius of the plot, in contradiction with the CV measurements. Other depositions do not change drastically the shape of the plot, with a dominant semi-infinite linear diffusion behavior, leading also to incoherent results as compared to CV curves. In the case of the protocol 2 (Figure 5e), EIS and CV measurements are in agreement, the first layer of streptavidin inducing in EIS plot a decrease of the resistance from approximately 5 kΩ with the bare electrode to 0.5 kΩ in the presence of streptavidin. The presence of the antibody layer has an opposite effect, increasing the resistance to approximately 0.8 kΩ. Such effects are coherent with current variations observed in CV curves.

At last, with the protocol 3 shown in Figure 5f, the presence of the streptavidin layer induces first an increase of the resistance which is doubled as compared to the bare electrode. The immobilization of the antibodies leads to an opposite effect. These results support those obtained by CV measurements.

Taking into account CV and EIS measurements, we can conclude that the most effective, reproducible and coherent electrochemical response was obtained when applying protocol 3 based on direct adsorption of the streptavidin molecule on the electroactive surface [36].

Focusing on these relevant results, we carried out a further characterization of the electrode functionalized according to the protocol 3 by FTIR spectroscopy to ensure the effectiveness of streptavidin coupling on the gold surface. We focused on the 3000-2600cm^{-1} range, where it is

possible to observe symmetrical and asymmetric stretching vibrations of methylene groups [37, 38], widely present in amino acids. As shown in Figure 6, the bare gold electrode surface gives no vibrational band in this range, unlike the streptavidin layer that induces the presence of characteristic bands at 2920 and 2850 cm^{-1}, which is consistent with effective deposit of this molecule.

Consequently, comparing the previous results in terms of efficiency and reproducibility, we focused our attention on protocols 2 and 3.

3.3 AFB1 detection

Once the protocols were chosen, we performed the final step of the characterization: functionalized gold electrodes were incubated with AFB1 solutions at concentrations ranging from 50 fg/ml to 10 ng/ml. AFB1 concentrations were multiplied by 10 from one test to another and a TBS rinsing step was included between each test. Different times of incubation ranging from 15 min to 45 min were tested. The most stable and reproducible signal was obtained after 30 min, which was then considered as optimal.

Despite the apparent efficiency of the protocol 2 illustrated by the modifications of the CV curves (Figure 5b), the corresponding electrodes did not show a sensitive response for the detection of AFB1: electrochemical responses were weak and saturation of the signal was rapidly reached with a low AFB1 concentration (50 pg/ml) (data not shown).

CV curves corresponding to protocol 3 are shown in Figure 7a, with a zoom at the top of the oxidation peak in Figure 7b. Successive increases in the AFB1 concentration induce a gradual increase in the oxidation current and the absolute value of the reduction one, which is probably due to the direct interaction between the antibody and its target molecule, the sensor's response being saturated at a concentration of 5 ng/ml of AFB1. The intensity of the oxidation current is reported as a function of the AFB1 concentration in Figure 7c, showing a linear relationship between these two parameters in the concentration range tested here. It should be noted that this linear behavior has been observed for more than a dozen tested sensors, which shows the reproducibility of these measurements and their robustness. In the case of the oxidation current (Figure 7c), the curve has an average slope of almost 18µA/ng.ml^{-1} and a limit of detection (LOD) of 50 fg/ml. This latter value was obtained using the formula (LOD = 3 * Standard deviation of blank/ Slope) [19].

The high sensitivity recorded for this sensor is mainly attributed to the fact that the electrical internal parameters of the homemade potentiostat are numerically amplified. Also, the cleaning process helped to activate more than 80 % of the electroanalytical surface. In addition, the high sensitivity could be due to the supramolecular interaction between SA and biotin that helps to amplify the signal and to keep stable interactions since forces between these two molecules are considered one of the strongest and tightest bonds (dissociation factor is about 10^{-15}M). Also, biotinylated antibodies, once bound with SA, can maintain their immunological reactivity and, interactions with their specific antigen become more stable and enhanced [39].

The performance of our sensor was compared to that of other AFB1 sensors already described in the literature from their LODs since this parameter simply defines the performance of biosensors and it is easily comparable. The diagram presented in Figure 8 describes the evolution of this parameter over the last three years (2015-2018) [40-53]: the LOD of AFB1 sensors has considerably decreased in 2016 and 2017. However, to our knowledge, our sensor is one of the most efficient with the lowest LOD value, confirming the efficiency of the protocol 3 for the functionalization of the electrode. These performances can be explained by the appropriate orientation of the anti-AFB1 antibody, promoting an efficient interaction with the toxin and an enhancement of electron transfer at the surface of the electrode, associated with the stability of the whole molecular architecture (streptavidin/biotinylated-antibody/toxin). Finally, our sensor could be an effective solution to detection issues related to the low molecular weight of AFB1.

At last, to validate the applicability of the proposed method, our immunosensor for AFB1 was applied to the detection by CV measurements of this toxin in rice milk samples. Figure 9 shows for instance the values of oxidation current measured when increasing the concentration of AFB1 in 0.5 pg/ml increments from 1.0 to 2.5 pg/ml . As shown in Figure 9, an increase of the concentration leads as expected to a more accurate detection. The current regularly and reproducibly increases with AFB1 concentration with a positive linear correlation of about 0.95, although the variation of the current is not important,. This last point could be related to the viscosity and complexity of the samples. Nevertheless, despite the weak recorded current variations observed for this complex sample, our sensor allowed the acquisition of accurate measurements with an average recovery of almost 27% (± 3.3 SD).

4. Conclusion:

In this work, we have developed and characterized a novel electrochemical immunosensor based on screen-printing technology for the detection of fungal AFB1 toxin. A simple process of functionalization of gold electrodes led to the formation of stable surfaces allowing efficient adsorption of the anti-AFB1 antibody followed AFB1 detection characterized by a sensitivity of 18 $\mu A/ng.ml^{-1}$ and a LOD of 50 fg/ml. This last value shows that our sensor is highly competitive compared to other sensors developed for the same purpose. These results also highlight the undeniable advantage of the combination of different tools of physical chemistry, biochemistry, microfluidics and electronics. Such an approach could easily be applied to the design of sensors for detection of other target molecules by simply changing the nature of the antibody.

Funding: This research did not receive any specific grant from funding agencies in the public, commercial, or not-for-profit sectors.

References

[1] K. Carlson, M. Misra, S. Mohanty, Developments in micro- and nanotechnology for foodborne pathogen detection, Foodborne Pathog. Dis. 15 (2018) 16–25. doi:10.1089/fpd.2017.2309.

[2] V. Velusamy, K. Arshak, O. Korostynska, K. Oliwa, C. Adley, An overview of foodborne pathogen detection: In the perspective of biosensors, Biotechnol. Adv. 28 (2010) 232–254. doi:10.1016/j.biotechadv.2009.12.004.

[3] K. De Ruyck, M. De Boevre, I. Huybrechts, S. De Saeger, Dietary mycotoxins, co-exposure, and carcinogenesis in humans: short review, Mutat. Res. Mutat. Res. 766. (2015) 32–41. doi: 10.1016/j.mrrev.2015.07.003

[4] J.N. Selvaraj, Y. Wang, L. Zhou, Y. Zhao, F. Xing, X. Dai, Y. Liu, Recent mycotoxin survey data and advanced mycotoxin detection techniques reported from China: a review, Food Addit. Contam. Part A. 32 (2015) 440–452. doi:10.1080/19440049.2015.1010185.

[5] M. Edite Bezerra da Rocha, F. da Chagas Oliveira Freire, F. Erlan Feitosa Maia, M. Izabel Florindo Guedes, D. Rondina, Mycotoxins and their effects on human and animal health, Food Control 36. (2014) 159–165. doi: 10.1016/j.foodcont.2013.08.021

[6] A. Karczmarczyk, A.J. Baeumner, K.-H. Feller, Rapid and sensitive inhibition-based assay for the electrochemical detection of Ochratoxin A and Aflatoxin M1 in red wine and milk, Electrochimica Acta. 243 (2017) 82–89. doi:10.1016/j.electacta.2017.05.046.

[7] H.P. Dwivedi, L.-A. Jaykus, Detection of pathogens in foods: the current state-of-the-art and future directions, Crit. Rev. Microbiol. 37. (2011) 40–63. doi: 10.3109/1040841X.2010.506430

[8] S. Marchese, A. Polo, A. Ariano, S. Velotto, S. Costantini, L. Severino, Aflatoxin B1 and M1: Biological properties and their involvement in cancer development, Toxins 10. (2018) 1–19. doi: 10.3390/toxins10060214

[9] IARC Working Group Reports, Human exposure to aflatoxins and fumonisins, in: Mycotoxin control low- middle-income Ctries., International Agency for Research on Cancer, 2015: pp. 1–5.

[10] D. Pan, G. Li, H. Hu, H. Xue, M. Zhang, M. Zhu, X. Gong, Y. Zhang, Y. Wan, Y. Shen, Direct immunoassay for facile and sensitive detection of small molecule aflatoxin B_1 based on nanobody, Chem. - Eur. J. 24 (2018) 9869–9876. doi:10.1002/chem.201801202.

[11] L. Wang, F. Zhu, M. Chen, Y. Zhu, J. Xiao, H. Yang, X. Chen, Rapid and visual detection of aflatoxin B1 in foodstuffs using aptamer/G-quadruplex DNAzyme probe with low background noise, Food Chem. 271 (2019) 581–587. doi:10.1016/j.foodchem.2018.08.007.

[12] J. Moon, J. Byun, H. Kim, E.-K. Lim, J. Jeong, J. Jung, T. Kang, On-site detection of aflatoxin B1 in grains by a palm-sized surface plasmon resonance sensor, Sensors. 18 (2018) 598. doi:10.3390/s18020598.

[13] F. Di Nardo, E. Alladio, C. Baggiani, S. Cavalera, C. Giovannoli, G. Spano, L. Anfossi, Colour-encoded lateral flow immunoassay for the simultaneous detection of aflatoxin B1 and type-B fumonisins in a single Test line, Talanta. 192 (2019) 288–294. doi:10.1016/j.talanta.2018.09.037.

[14] F. Arduini, S. Cinti, V. Caratelli, L. Amendola, G. Palleschi, D. Moscone, Origami multiple paper-based electrochemical biosensors for pesticide detection, Biosens. Bioelectron. 126 (2019) 346–354. doi:10.1016/j.bios.2018.10.014.

[15] O.O. Olaoye, R. A., R. A. Manderville, Aptamer utility in sensor platforms for the detection of toxins and heavy metals, J. Toxins 4. (2017) 1–12.

[16] S.-H. Cao, Z.-R. Ni, L. Huang, H.-J. Sun, B. Tang, L.-J. Lin, Y.-Q. Huang, Z.-Y. Zhou, S.-G. Sun, Z. Chen, In situ monitoring potential-dependent electrochemical process by liquid NMR spectro-electrochemical determination: A Proof-of-Concept Study, Anal. Chem. 89. (2017) 3810–3813. doi: 10.1021/acs.analchem.7b00249

[17] K. Hsieh, S.B. Ferguson, M. Eisenstein, K.W. Plaxco, T.H. Soh, Integrated electrochemical microsystems for genetic detection of pathogens at the point of care, Acc. Chem. Res. 48. (2015) 911−920. doi: 10.1021/ar500456w

[18] A.F.D. Cruz, N. Norena, A. Kaushik, S. Bhansali, A low-costminiaturized potentiostat for point-of-care diagnosis, Biosens. Bioelectron. 62. (2015) 249–254.doi: 10.1016/j.bios.2014.06.053

[19] M.G.R. Pimenta-Martins, R.F. Furtado, L.G.D. Heneine, R.S. Dias, M. de F. Borges, C.R. Alves, Development of an amperometric immunosensor for detection of staphylococcal enterotoxin type A in cheese, J. Microbiol. Methods 91. (2012) 138–143. doi: 10.1016/j.mimet.2012.05.016

[20] K. Grennan, A.J. Killard, M.R. Smyth, Physical characterizations of a screen-printed electrode for use in an amperometric biosensor system, Electroanal. 13. (2001) 745–750. doi: 10.1002/1521-4109(200105)13:8/9<745::AID-ELAN745>3.0.CO;2-B

[21] A.J. Bandodkar, J. Wang, Non-invasive wearable electrochemical sensors: a review, Trends Biotechnol. 32. (2014) 363–371. doi: 10.1016/j.tibtech.2014.04.005

[22] L. Guo, J. Feng, Z. Fang, J. Xu, X. Lu, Application of microfluidic “lab-on-a-chip” for the detection of mycotoxins in foods, Trends Food Sci. Technol. (2015) 1–12. doi: 10.1016/j.tifs.2015.09.005

[23] M. Tudorache, C. Bala, Biosensors based on screen-printing technology, and their applications in environmental and food analysis, Anal Bioanal Chem 388. (2007) 565–578. doi: 10.1007/s00216-007-1293-0

[24] C. Dincer, R. Bruch, A. Kling, P.S. Dittrich, G. A.Urban, Multiplexed point-of-care testing – xPOCT, Trends Biotechnol. 35. (2017) 728–742. doi: 10.1016/j.tibtech.2017.03.013

[25] P. Mehrotra, Biosensors and their applications – A review, J. Oral Biol. Craniofacial Res. 6 (2016) 153–159. doi:10.1016/j.jobcr.2015.12.002.

[26] L.M. Fischer, M. Tenje, A.R. Heiskanen, N. Masuda, J. Castillo, A. Bentien, J. Émneus, M.H. Jakobsen, A. Boisen, Gold cleaning methods for electrochemical detection applications, Microelectron. Eng. 86 (2009) 1282–1285. doi:10.1016/j.mee.2008.11.045.

[27] O.H. Laitinen, H.R. Nordlund, V.P. Hytönen, M.S. Kulomaa, Brave new (strept)avidins in biotechnology, Trends Biotechnol. 25 (2007) 269–277. doi:10.1016/j.tibtech.2007.04.001.

[28] E.P. Diamand, T.K. Christopoulos, The biotin-(strept)avidin system: Principles and applications in biotechnology, Clin. Chem. 37. (1991) 625–638.

[29] A. Sharma, G. Catanante, A. Hayat, G. Istamboulie, I. Ben Rejeb, S. Bhand, J.L. Marty, Development of structure switching aptamer assay for detection of aflatoxin M1 in milk sample, Talanta. 158 (2016) 35–41. doi:10.1016/j.talanta.2016.05.043.

[30] Z. Ben Abdallah, I. Gammoudi, M. Ben Ismail, M. Mathelié-Guinlet, F. Morote, S. Cassagnere, R. Boigard, A. Othmane, H. Sghaier, T. Cohen-Bouhacina, Development of a new integrated easy to use micro-electrochemical platform for food analysis and staphylococcal enterotoxin B detection, Procedia Eng. 168. (2016) 1609–1612. doi:10.1016/j.proeng.2016.11.472.

[31] S.-J. Ding, B.-W. Chang, C.-C. Wu, M.-F. Lai, H.-C. Chang, Electrochemical evaluation of avidin–biotin interaction on self-assembled gold electrodes, Electrochimica Acta. 50 (2005) 3660–3666. doi:10.1016/j.electacta.2005.01.011.

[32] E.B. Bahadır, M.K. Sezgintürk, A review on impedimetric biosensors, Artif. Cells Nanomedicine Biotechnol. 44 (2016) 248–262. doi:10.3109/21691401.2014.942456.

[33] B.T. Adeyemo, L.O. Tiamiyu, V.O. Ayuba, S. Musa, J. Odo, Effects of dietary mixed aflatoxin B1 and fumonisin B1 on growth performance and haematology of juvenile Clarias gariepinus catfish, Aquaculture. 491 (2018) 190–196. doi:10.1016/j.aquaculture.2018.03.026.

[34] R. D'Agata, P. Palladino, G. Spoto, Streptavidin-coated gold nanoparticles: critical role of oligonucleotides on stability and fractal aggregation, J. Nanotechnol. 8. (2017) 1–11. doi: 10.3762/bjnano.8.1

[35] P. Kalita, J. Singh, M.K. Singh, P.R. Solanki, G. Sumana, B.D. Malhotra, Ring like self-assembled Ni nanoparticles based biosensor for food toxin detection, Appl. Phys. Lett. 100. (2012) 093702_2-093702_4. doi: 10.1063/1.3690044

[36] H. Kuramitz, K. Sugawara, S. Tanaka, Electrochemical sensing of avidin-biotin interaction using redox markers, Electroanalysis. 12 (2000) 1299–1303. doi:10.1002/1521-4109(200011)12:16<1299::AID-ELAN1299>3.0.CO;2-6.

[37] A. Adamiano, S. Goffredo, Z. Dubinsky, O. Levy, S. Fermani, D. Fabbri, G. Falini, Analytical pyrolysis-based study on intra-skeletal organic matrices from Mediterranean corals, Anal Bioanal Chem 406. (2014) 6021–6033. doi: 10.1007/s00216-014-7995-1

[38] V. Parravicini, E. Smidt, K. Svardal, H. Kroiss, Evaluating the stabilisation degree of digested sewage sludge: investigations at four municipal wastewater treatment plants, Water Sci. Technol. 53. (2006) 81–90.

[39] H. Schetters, Avidin and streptavidin in clinical diagnostics, Biomol. Eng. 16 (1999) 73–78.

[40] T. Sergeyeva, D. Yarynka, E. Piletska, R. Lynnik, O. Zaporozhets, O. Brovko, S. Piletsky, A. El'skaya, Fluorescent sensor systems based on nanostructured polymeric membranes for selective recognition of Aflatoxin B1, Talanta. 175 (2017) 101–107. doi:10.1016/j.talanta.2017.07.030.

[41] J. Zhang, Z. Li, S. Zhao, Y. Lu, Size-dependent modulation of graphene oxide–aptamer interactions for an amplified fluorescence-based detection of aflatoxin B $_1$ with a tunable dynamic range, The Analyst. 141 (2016) 4029–4034. doi:10.1039/C6AN00368K.

[42] B. Wang, Y. Chen, Y. Wu, B. Weng, Y. Liu, Z. Lu, C.M. Li, C. Yu, Aptamer induced assembly of fluorescent nitrogen-doped carbon dots on gold nanoparticles for sensitive detection of AFB 1, Biosens. Bioelectron. 78 (2016) 23–30. doi:10.1016/j.bios.2015.11.015.

[43] L. Chen, F. Wen, M. Li, X. Guo, S. Li, N. Zheng, J. Wang, A simple aptamer-based fluorescent assay for the detection of Aflatoxin B1 in infant rice cereal, Food Chem. 215 (2017) 377–382. doi:10.1016/j.foodchem.2016.07.148.

[44] Y. Seok, J.-Y. Byun, W.-B. Shim, M.-G. Kim, A structure-switchable aptasensor for aflatoxin B1 detection based on assembly of an aptamer/split DNAzyme, Anal. Chim. Acta. 886 (2015) 182–187. doi:10.1016/j.aca.2015.05.041.

[45] H. Ma, J. Sun, Y. Zhang, C. Bian, S. Xia, T. Zhen, Label-free immunosensor based on one-step electrodeposition of chitosan-gold nanoparticles biocompatible film on Au microelectrode for determination of aflatoxin B 1 in maize, Biosens. Bioelectron. 80 (2016) 222–229. doi:10.1016/j.bios.2016.01.063.

[46] H. Ma, J. Sun, Y. Zhang, S. Xia, Disposable amperometric immunosensor for simple and sensitive determination of aflatoxin B 1 in wheat, Biochem. Eng. J. 115 (2016) 38–46. doi:10.1016/j.bej.2016.08.003.

[47] K.Y. Goud, A. Hayat, G. Catanante, S. M., K.V. Gobi, J.L. Marty, An electrochemical aptasensor based on functionalized graphene oxide assisted electrocatalytic signal amplification of methylene blue for aflatoxin B1 detection, Electrochimica Acta. 244 (2017) 96–103. doi:10.1016/j.electacta.2017.05.089.

[48] A. Krittayavathananon, M. Sawangphruk, Impedimetric sensor of ss-HSDNA/reduced graphene oxide aerogel electrode toward Aflatoxin B1 detection: Effects of redox mediator charges and hydrodynamic diffusion, Anal. Chem. 89 (2017) 13283–13289. doi:10.1021/acs.analchem.7b03329.

[49] X. Zhou, S. Wu, H. Liu, X. Wu, Q. Zhang, Nanomechanical label-free detection of aflatoxin B1 using a microcantilever, Sens. Actuators B Chem. 226 (2016) 24–29. doi:10.1016/j.snb.2015.11.092.

[50] R. Chauhan, J. Singh, P.R. Solanki, T. Manaka, M. Iwamoto, T. Basu, B.D. Malhotra, Label-free piezoelectric immunosensor decorated with gold nanoparticles: Kinetic analysis and biosensing application, Sens. Actuators B Chem. 222 (2016) 804–814. doi:10.1016/j.snb.2015.08.117.

[51] K. Abnous, N.M. Danesh, M. Alibolandi, M. Ramezani, A. Sarreshtehdar Emrani, R. Zolfaghari, S.M. Taghdisi, A new amplified π-shape electrochemical aptasensor for ultrasensitive detection of aflatoxin B 1, Biosens. Bioelectron. 94 (2017) 374–379. doi:10.1016/j.bios.2017.03.028.

[52] J. Chen, J. Wen, L. Zhuang, S. Zhou, An enzyme-free catalytic DNA circuit for amplified detection of aflatoxin B1 using gold nanoparticles as colorimetric indicators, Nanoscale. 8 (2016) 9791–9797. doi:10.1039/C6NR01381C.

[53] A. Li, L. Tang, D. Song, S. Song, W. Ma, L. Xu, H. Kuang, X. Wu, L. Liu, X. Chen, C. Xu, A SERS-active sensor based on heterogeneous gold nanostar core–silver nanoparticle satellite assemblies for ultrasensitive detection of aflatoxin B1, Nanoscale. 8 (2016) 1873–1878. doi:10.1039/C5NR08372A.

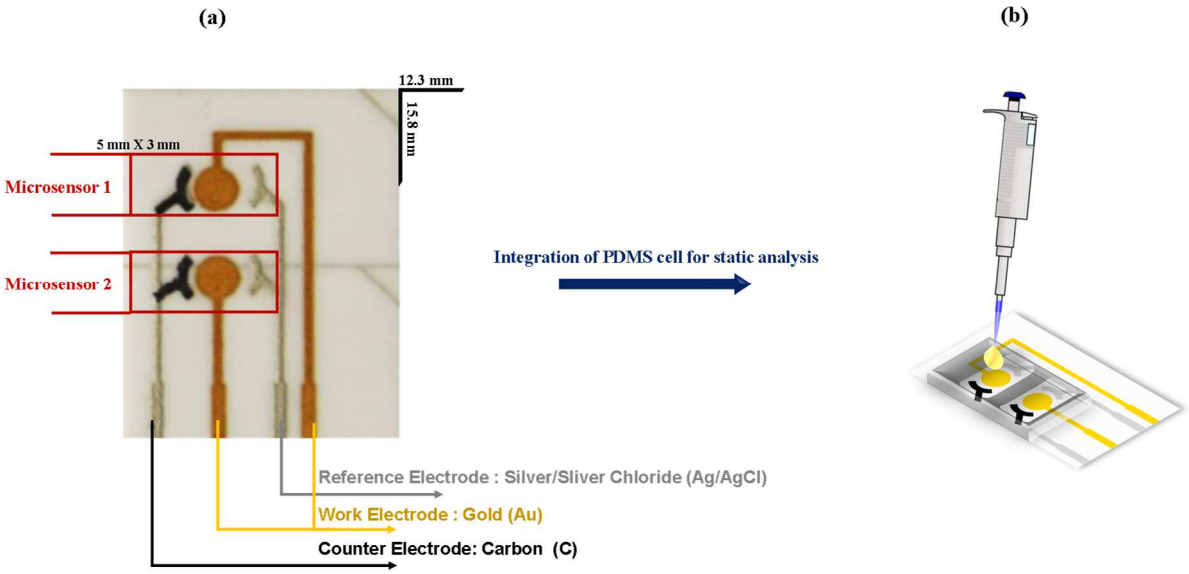

Figure 1: (a) Organization and dimensions of electrodes in our homemade microchip and presentation of the final product; (b) Schematic representation of the microchip and the PDMS static cells.

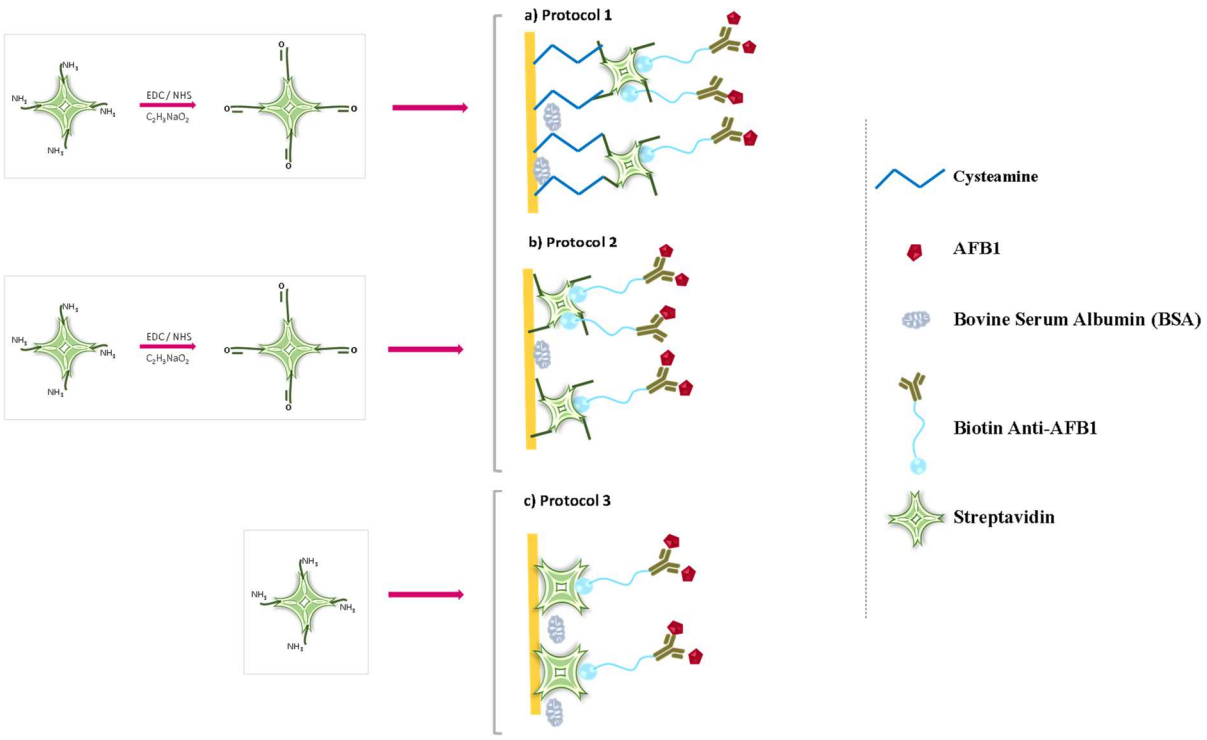

570

571 **Figure 2**: Description of the three functionalization protocols studied in this work.

572

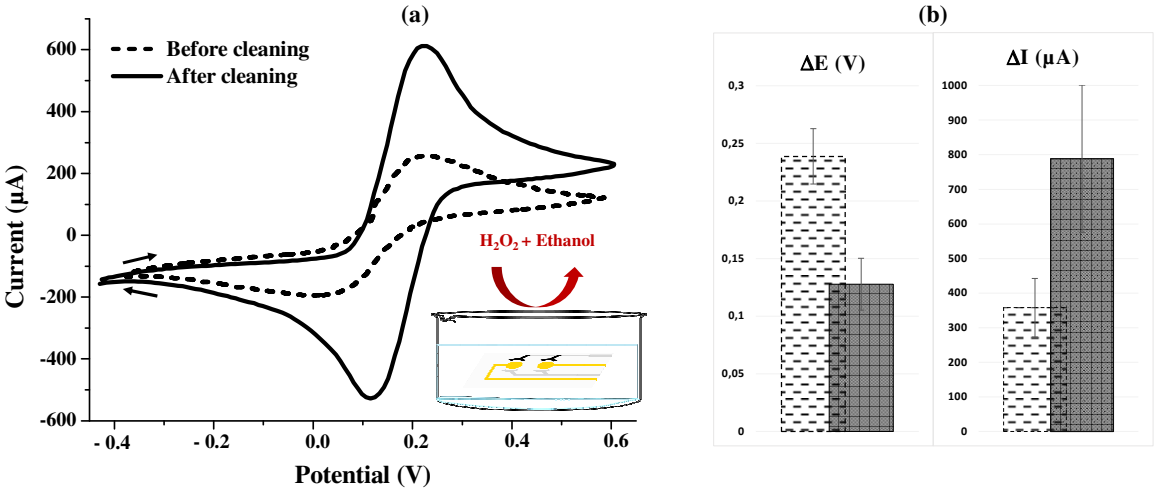

Figure 3: (a) CV curves obtained with the gold electrode in contact with the redox couple solution before and after the cleaning process; (b) Increase of current and potential's gap after the cleaning process (error bars correspond to standard deviation for five independent sensors).

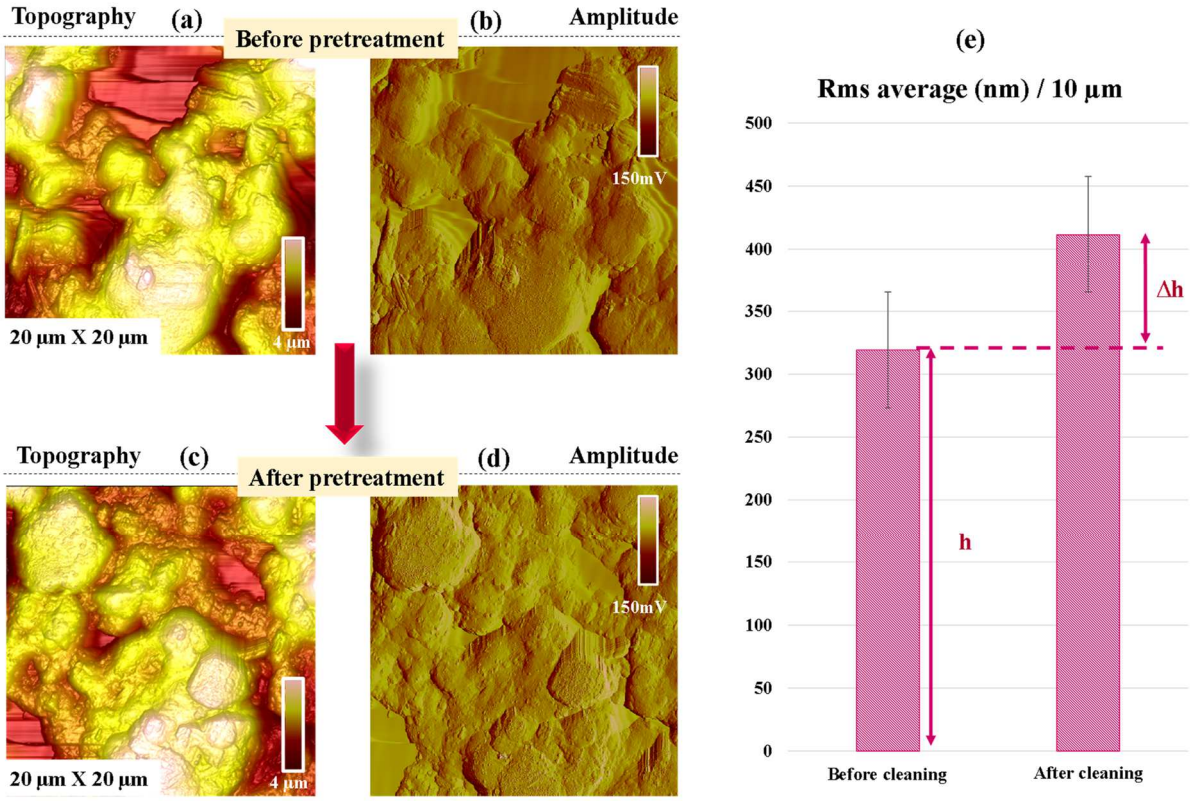

Figure 4: AFM height (a, c) and amplitude (b, d) images of a gold electrode surface (a, b) before and (c, d) after the cleaning process, and (e) histogram showing the Root Mean Square roughness (Rms) variation between the surfaces before and after the cleaning.

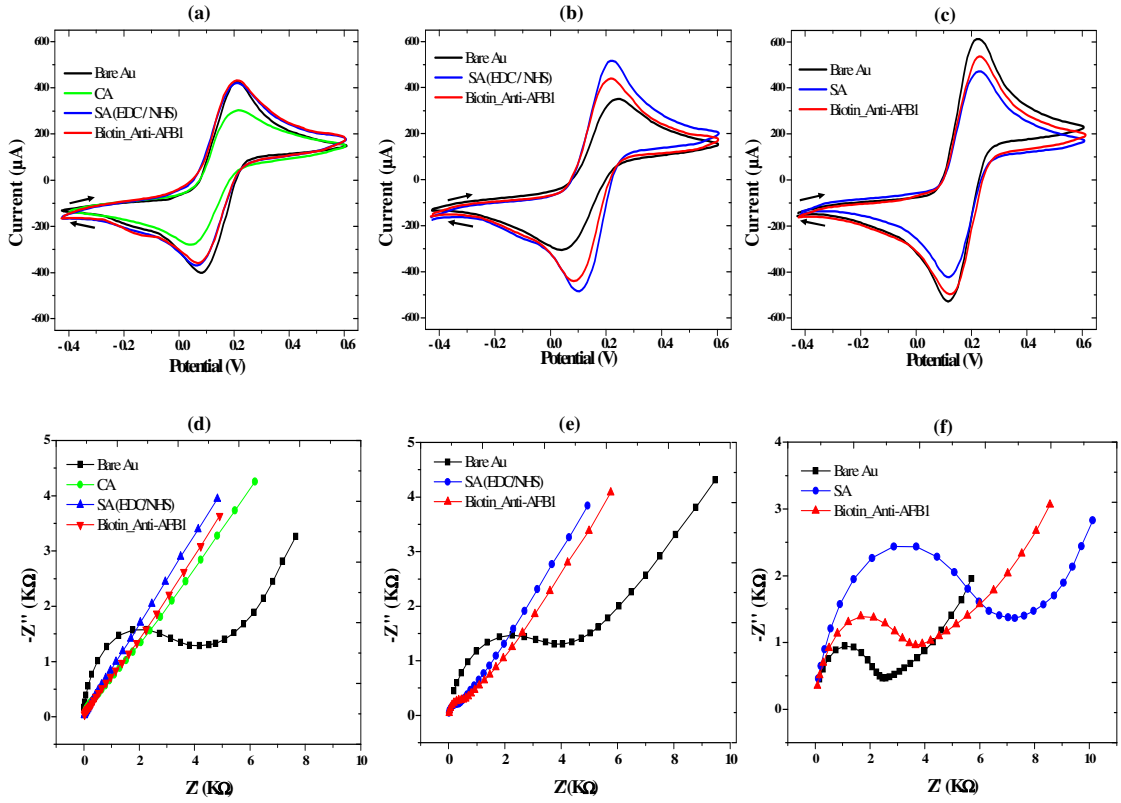

Figure 5: CV (a, b, c) and EIS (d, e, f) diagrams of gold electrodes functionalized following one of the three protocols: (a, d) protocol 1 (Au/CA/SA(EDC/NHS)/Biotin_Anti-AFB1); (b, e) protocol 2 (Au/SA(EDC/NHS)/Biotin_Anti-AFB1); (c, f) protocol 3 (Au/SA/Biotin_Anti-AFB1).

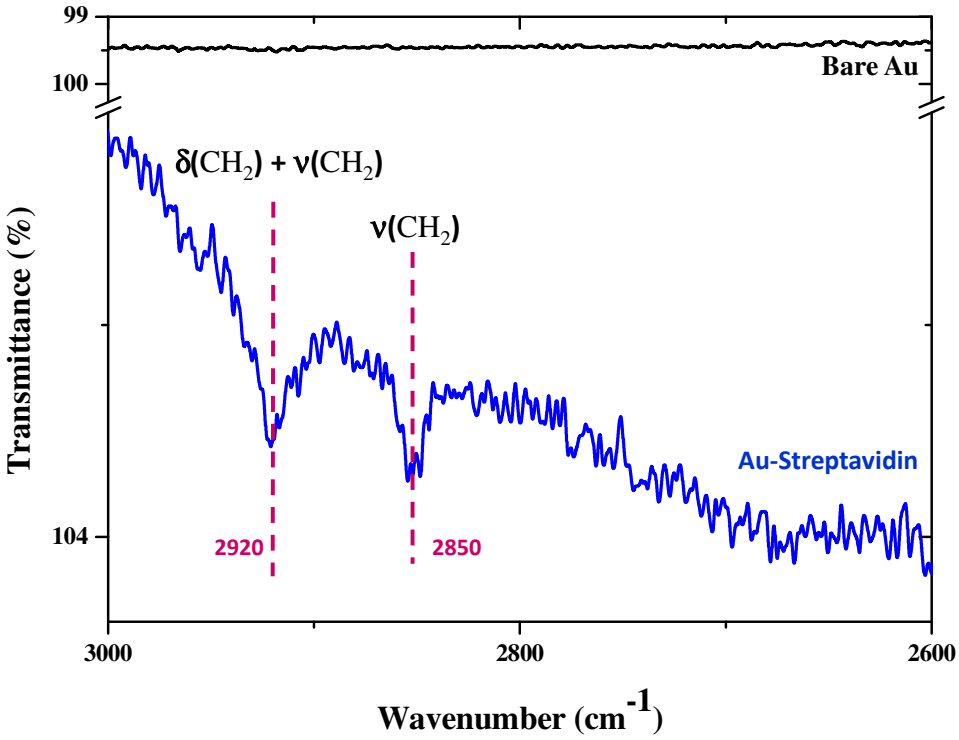

607

608 **Figure 6:** FTIR spectra in the 3000-2600 cm^{-1} range of a bare gold electrode and a gold
609 electrode functionalized with streptavidin following protocol 3 (direct adsorption).

610

611

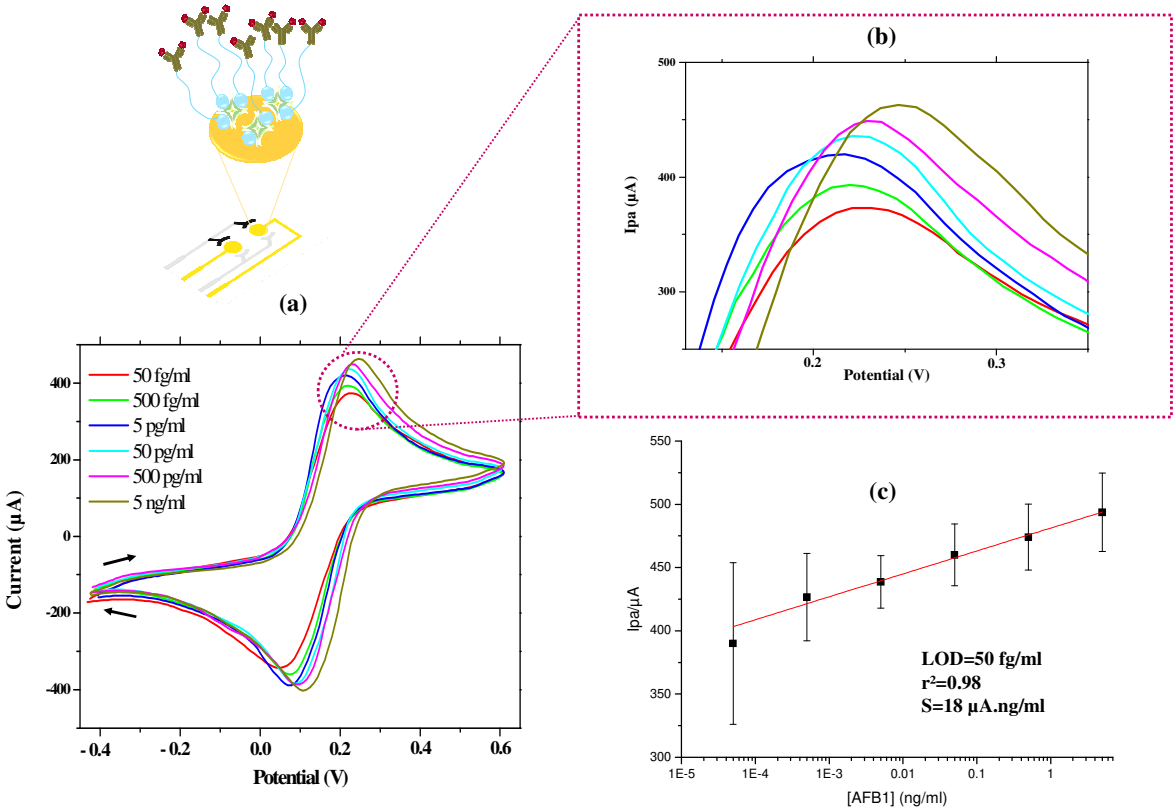

612

613 **Figure 7:** (a) CV curves corresponding to AFB1 detection (using the protocol 3) within a
614 concentration range between 50 fg/ml and 5 ng/ml; (b) Zoom at the top of the oxidation peak
615 showing the gradual increase of the oxidation current (I_{pa}) ; (c) Calibration curve based on the
616 oxidation current.

617

618

619

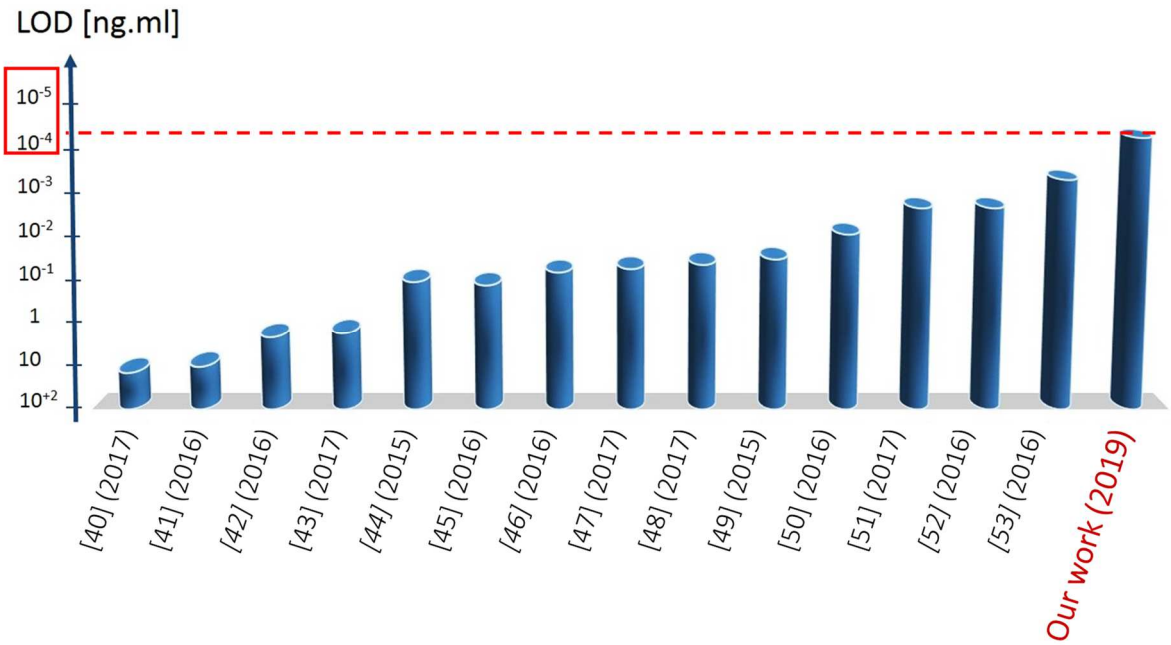

620

621 **Figure 8:** LOD values of different sensors designed for the detection of AFB1 for the 2015-
622 2018 period compared with the performance of the sensor developed in this work.
623 Corresponding references are indicated.

624

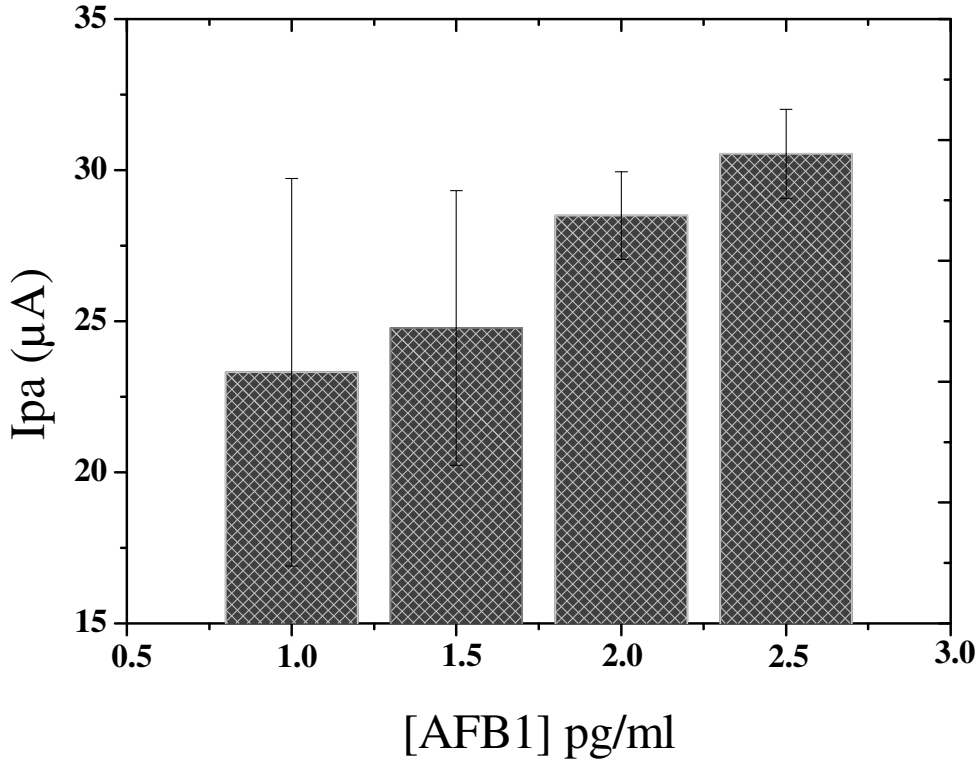

625

626 **Figure 9:** Oxidation current histograms while the detection of AFB1 in rice milk using
627 cumulative successive addition of 500 fg/ml

Graphical abstract